CO oxidation at Pd(100): A first-principles constrained thermodynamics study

Jutta Rogal, Karsten Reuter, and Matthias Scheffler

Fritz-Haber-Institut der Max-Planck-Gesellschaft, Faradayweg 4-6, D-14195 Berlin, Germany

(Received 30 January 2007; published 23 May 2007)

The possible formation of oxides or thin oxide films (surface oxides) on late transition-metal surfaces has recently been recognized as an essential ingredient when aiming to understand catalytic oxidation reactions under technologically relevant gas phase conditions. Using CO oxidation at Pd(100) as an example, we investigate the composition and structure of this model catalyst surface over a wide range of (T,p) conditions within a multiscale modeling approach where density-functional theory is linked to thermodynamics. The results show that under the catalytically most relevant gas phase conditions a thin surface oxide is the most stable "phase" and that the system is actually very close to a transition between this oxidic state and a reduced state in terms of a CO-covered Pd(100) surface.

I. INTRODUCTION

Catalytic oxidation using transition metals (TMs) as the active material is an important technological process, of which we have still only limited microscopic insight. Much valuable microscopic information that has been obtained under ultrahigh-vacuum (UHV) conditions is not directly transferable to the conditions of practical catalysis (with pressures of several bars and elevated temperatures). And *in-situ* techniques that would operate under these conditions are still struggling to achieve atomic-scale surface sensitive information. A key factor that hinders the direct transfer of the insight gained under UHV conditions is that under reaction conditions the entire structure and composition of the catalyst surface might be changed (often called the "materials gap"). And if a new material is created during the induction period of the catalytic process, it will obviously exhibit a very different chemical activity; it will be quantitatively and even qualitatively different. Under the oxygen-rich gas phase conditions and elevated temperatures of oxidation catalysis the surface of the transition metal catalyst might, e.g., be oxidized, so that the actual catalytically active state is not the pristine metal, but rather the formed oxide. One example for this is the CO oxidation reaction over ruthenium. Here it was found that under UHV conditions the Ru(0001) model catalyst shows almost no catalytic activity, whereas under high oxygen pressures its catalytic activity exceeds even the one of the frequently used palladium and platinum catalysts.[1] This increase in the catalytic activity was traced back to the formation of a RuO_2 film at the surface.[2,3] For the ruthenium catalyst a clear distinction could thus be made between the different states: namely, the weakly catalytically active metal under low oxygen pressures and the highly active oxide film under high oxygen pressures.

For the model system discussed here, the CO oxidation at Pd(100), recent *in-situ* experimental measurements also indicate that an oxidic structure at the Pd(100) surface might be formed under gas phase conditions applied in industrial oxidation catalysis. Using surface x-ray diffraction (SXRD) measurements a (T,p) diagram showing the detected structures in a pure oxygen atmosphere over a temperature range of $T=600-1000$ K and pressures of $p_{O_2}=10^{-9}-1$ atm could

be inferred.[4] A thin surface oxide structure was measured over an extended (T,p) range, suggesting that this structure might also appear under catalytic reaction conditions. In reactor scanning tunneling microscopy (STM) experiments by Hendriksen *et al.*[5,6] the structure of the Pd(100) surface could be directly monitored during the catalytic oxidation of CO. Here, the surface was exposed to both oxygen and CO at a total pressure of $p_{tot} \approx 1$ atm and a temperature of $T \approx 400$ K. The partial pressures of the reactant gases CO and O_2, as well as the reaction product CO_2, were measured simultaneously with the STM images. Depending on the partial pressure ratio of O_2 and CO the authors observed a change in the reaction rate, which was accompanied by a significant change in the morphology of the surface. This morphology change (albeit not atomically resolved) was interpreted as a change from the adsorbate-covered Pd(100) surface to an oxidic state.

To address this problem from a theoretical point of view we employ a multiscale modeling approach where we use density-functional theory (DFT) to describe the system on an electronic (microscopic) level. By linking these results to thermodynamics[7–10] it becomes possible to address much larger system sizes and to compare the stability of different surface structures in contact with the surrounding gas phase.[11–16] We use in particular a *constrained* equilibrium approach,[15,16] where the surface is considered to be in full thermodynamic equilibrium with two separate gas phase reservoirs of O_2 and CO, and not allowing that O_2 and CO can react. The key result obtained is a surface "phase diagram," which provides first insight into possible surface structures over a wide range of temperature and pressure conditions of the O_2 and CO gas phase. Focusing on gas phase conditions relevant for oxidation catalysis we find the system on the verge of either stabilizing a thin surface oxide structure or a CO-covered Pd(100) surface. It is thus well possible and even likely that the surface oxide structure contributes to the active state of the Pd(100) model catalyst under reaction conditions. However, to verify this, the kinetic effects of the ongoing catalytic CO_2 formation need to be considered. This is done in a second step of our hierarchical approach by performing kinetic Monte Carlo (kMC) simulations on the surface structures identified here, on which we report in a consecutive paper.

II. THEORY

A. Gibbs free energy of adsorption

To determine the stability of a surface in contact with a gas phase reservoir we use the surface free energy γ. For a multicomponent system in equilibrium with atomic reservoirs (e.g., a surrounding gas or liquid phase environment or a macroscopic bulk phase) a general expression for the surface free energy is given by

$$\gamma(T,\{p_i\}) = \frac{1}{A}\left[G^{\text{surf}} - \sum_i N_i \mu_i(T,p_i)\right]. \quad (1)$$

Here, G^{surf} is the Gibbs free energy of the solid including the surface, A is the surface area, and $\mu_i(T,p_i)$ are the chemical potentials of the various species i in the system. To compare the stability of different adsorption structures of oxygen and CO on the Pd(100) surface depending on the surrounding gas phase conditions one has to evaluate the Gibbs free energy of adsorption, ΔG^{ads}.[17,18] For this, the stability of the different adsorption structures is compared with respect to the clean metal surface. For a Pd(100) surface in a *constrained equilibrium* with an O_2 and CO gas phase ΔG^{ads} is thus given by

$$\Delta G^{\text{ads}}(\Delta\mu_O, \Delta\mu_{CO}) = \gamma_{\text{Pd}(100)} - \gamma_{O,CO@\text{Pd}(100)}$$

$$= -\frac{1}{A}[G^{\text{surf}}_{O,CO@\text{Pd}(100)} - G^{\text{surf}}_{\text{Pd}(100)}$$

$$- \Delta N_{\text{Pd}}\mu^{\text{bulk}}_{\text{Pd}} - N_O(1/2E^{\text{tot}}_{O_2} + \Delta\mu_O) - N_{CO}(E^{\text{tot}}_{CO} + \Delta\mu_{CO})]$$

$$\approx -\frac{1}{A}\widetilde{E}^{\text{bind}}_{O,CO@\text{Pd}(100)} + \frac{N_O}{A}\Delta\mu_O + \frac{N_{CO}}{A}\Delta\mu_{CO}, \quad (2)$$

where $G^{\text{surf}}_{O,CO@\text{Pd}(100)}$ is the Gibbs free energy of the Pd(100) surface, with N_O adsorbed O atoms and N_{CO} adsorbed CO molecules, and $G^{\text{surf}}_{\text{Pd}(100)}$ is the Gibbs free energy of the clean palladium surface. If the number of palladium atoms per surface area A in the adsorption structure, N_{Pd}, and in the clean surface, N'_{Pd}, are not equal (e.g., due to a surface reconstruction)—i.e., $\Delta N_{\text{Pd}} = N_{\text{Pd}} - N'_{\text{Pd}} \neq 0$—then the excess (deficiency) atoms are taken from (put into) a bulk reservoir, represented by the chemical potential of the bulk solid phase, $\mu^{\text{bulk}}_{\text{Pd}}$. The chemical potentials of the two gas phase reservoirs of oxygen, μ_{O_2}, and CO, μ_{CO}, have been separated into a total energy contribution and the remaining part containing all the temperature- and pressure-dependent terms—i.e., $\mu_O = 1/2\mu_{O_2} = 1/2E^{\text{tot}}_{O_2} + \Delta\mu_O(T,p)$, setting $\Delta\mu_O(T,p) = 1/2\Delta\mu_{O_2}(T,p)$ and $\mu_{CO} = E^{\text{tot}}_{CO} + \Delta\mu_{CO}(T,p)$.[13,16] In the last line of Eq. (2) the difference of the Gibbs free energies of the clean and adsorbate covered surfaces, and of the bulk system, has been approximated by the DFT total energies E.[13,16] A detailed discussion of the thereby neglected contributions to the Gibbs free energy of adsorption and their influence on the presented results will be given below.

In the constrained equilibrium approach leading to Eq. (2) the two gas phases are assumed to be noninteracting.[16] The Gibbs free energy of adsorption ΔG^{ads} depends then linearly on the chemical potentials of both the oxygen and CO gas phases. The slope is respectively determined by the surface

coverage of oxygen and/or CO. This is most apparent in the last line of Eq. (2), where we have introduced the average binding energy of O and CO as

$$\widetilde{E}^{\text{bind}}_{O,CO@\text{Pd}(100)} = \left(E^{\text{tot}}_{O,CO@\text{Pd}(100)} - E^{\text{tot}}_{\text{Pd}(100)} - \Delta N_{\text{Pd}}E^{\text{tot}}_{\text{Pd}} - \frac{N_O}{2}E^{\text{tot}}_{O_2}\right.$$

$$\left. - N_{CO}E^{\text{tot}}_{CO}\right). \quad (3)$$

Since the most stable structure will be the one with the lowest surface free energy, an adsorbate structure will be stable with respect to the clean surface if $\gamma_{O,CO@\text{Pd}(100)} < \gamma_{\text{Pd}(100)}$—i.e., if $\Delta G^{\text{ads}} > 0$. If two structures contain an equivalent amount of oxygen and CO, they will also show the same dependence on $\Delta\mu_O$ and $\Delta\mu_{CO}$. The ratio of how these two structures contribute to the stable structures is governed by the law of mass action, which enables us to directly exclude a less favorable structure if its binding energy $\widetilde{E}^{\text{bind}}_{O,CO@\text{Pd}(100)}$ differs by much more than k_BT from the one of the most favorable structure.

For the adsorption of O/CO on the Pd(100) surface the average binding energy defined in Eq. (3) is equivalent to the commonly used binding energy, which is often given per O atom or CO molecule, respectively—e.g., in the case of oxygen as

$$E^{\text{bind}}_{O@\text{Pd}(100)} = \frac{1}{N_O}\left(E^{\text{tot}}_{O@\text{Pd}(100)} - E^{\text{tot}}_{\text{Pd}(100)} - \frac{N_O}{2}E^{\text{tot}}_{O_2}\right). \quad (4)$$

In the case of additional adsorption of O (CO) on the reconstructed $\sqrt{5}$ surface oxide (which will be introduced below) the binding energy of the atom (molecule) with respect to this $\sqrt{5}$ structure is then given by (here exemplified for CO)

$$E^{\text{bind}}_{CO@\sqrt{5}} = \frac{1}{N_{CO}}\left(E^{\text{tot}}_{CO@\sqrt{5}} - E^{\text{tot}}_{\sqrt{5}} - N_{CO}E^{\text{tot}}_{CO}\right), \quad (5)$$

where $E^{\text{tot}}_{\sqrt{5}}$ is the total energy of the $\sqrt{5}$ surface oxide. We note that E^{bind} is in this case different from the above defined $\widetilde{E}^{\text{bind}}$ in Eq. (3), since the latter also contains the energetic changes due to the formation of the $\sqrt{5}$ surface oxide, i.e., it is referenced with respect to the clean Pd(100) surface.

B. Bulk oxide stability

When considering a metal surface in contact with an O_2 and CO gas phase complete conversion into an extended bulk oxide is also a thermodynamic possibility. The stability of the corresponding bulk oxide therefore has to be evaluated with respect to the two gas phase components and compared to the various stable structures forming at the metal surface.[18] A sufficient oxygen content in the gas phase will lead to the formation of bulk palladium oxide, PdO, whereas a sufficient CO content will favor the decomposition of PdO into CO_2 and Pd metal. In a pure oxygen gas phase the thermodynamic stability of the bulk oxide is given by

$$\mu^{\text{bulk}}_{\text{PdO}} < \mu^{\text{bulk}}_{\text{Pd}} + \mu_O, \quad (6)$$

whereas in a pure CO environment the stability condition for the oxide is

TABLE I. Computed heat of formation $\Delta H^f_{PdO}(0,0)$ and binding energies of O_2, CO and CO_2 (see text). The quoted experimental values are extrapolated to $T=0$ K, and the zero-point vibration energy (ZPE) has been removed. All values are in eV.

	PBE	RPBE	LDA	Expt.[a]	ZPE
ΔH^f_{PdO} (0,0)	−0.87	−0.62	−1.42	−0.97	
$E^{bind}_{O_2}$	−6.22	−5.75	−7.56	−5.30	(0.10)
E^{bind}_{CO}	−11.65	−11.20	−12.93	−11.33	(0.13)
$E^{bind}_{CO_2}$	−17.99	−17.09	−20.43	−16.98	(0.27)
ΔE^{mol}	−3.24	−3.02	−3.72	−3.00	

[a]Reference 20.

$$\mu^{bulk}_{PdO} + \mu_{CO} < \mu^{bulk}_{Pd} + \mu_{CO_2}. \tag{7}$$

If we approximate the chemical potential of the free CO_2 molecule by its total energy only,[18] Eqs. (6) and (7) can be combined, yielding the stability criterion for PdO in an oxygen- and CO-containing gas phase:

$$\Delta\mu_{CO} - \Delta\mu_O \lesssim -2\Delta H^f_{PdO}(T=0 \text{ K}) + \Delta E^{mol}. \tag{8}$$

Here, $\Delta H^f_{PdO} \approx E^{tot}_{PdO} - E^{tot}_{Pd} - 1/2 E^{tot}_{O_2}$ is the heat of formation of PdO at $T=0$ K and $\Delta E^{mol} = E^{bind}_{CO_2} - E^{bind}_{CO} - 1/2 E^{bind}_{O_2}$ is the difference in binding energies between the three gas phase molecules. Table I compiles these binding energies, as well as the heat of formation of PdO, as obtained by previously published highly converged DFT calculations[19] and using the computational methodology described below. In addition the experimental values are quoted. These values have been extrapolated to $T=0$ K, and the zero-point vibration energy (also listed in Table I) has been removed.

Substituting the chemical potential of CO_2, μ_{CO_2}, by only the total energy term $E^{tot}_{CO_2}$ in Eq. (7) is a rather crude approximation. The most important contributions that have been neglected arise from the vibrational and translational free energy. The assumption that the CO_2 formed at the surface is readily transported away motivates us to disregard the translational free energy contribution as we discussed in more detail in Ref. 18. The vibrational free energy contribution will be of the order of the ZPE for the temperature range discussed here. As can be seen in Table I the ZPE value for CO_2 is approximately 0.3 eV. Variations of ΔE^{mol} in Eq. (8) of this order of magnitude do not affect any of the conclusions discussed below, which justifies the rather crude approximation for the present purpose.

C. Computational setup

With the approximations made in the last two subsections, the crucial quantities determining the stability of surface structures are the total energies of the extended surfaces and of the involved gas phase molecules. These total energies are obtained by DFT calculations which have been performed within the full-potential (linearized) augmented plane wave + local orbital (L)APW+lo method[21,22] as implemented in the WIEN2k code.[23]

All surfaces are simulated within the supercell approach using inversion-symmetric slabs consisting of five Pd(100) layers with adsorption of oxygen and/or CO or the reconstructed surface oxide plus additional O/CO on both sides. The vacuum between consecutive slabs is at least 14 Å. The adsorption layers and two outermost palladium layers have been fully relaxed. The muffin-tin radii have been set to $R^{Pd}_{MT} = 2.0$ bohr for palladium, $R^O_{MT} = 1.0$ bohr for oxygen, and $R^C_{MT} = 1.0$ bohr for carbon. Inside the muffin-tins the wave functions are expanded up to $l^{wf}_{max} = 12$ and the potential up to $l^{pot}_{max} = 6$. For the Pd(100)-(1×1) structure a $[10 \times 10 \times 1]$ Monkhorst-Pack (MP) grid has been used to integrate the Brillouin zone (BZ). For larger surface unit cells the MP grid has been reduced accordingly to assure an equivalent sampling of the BZ. Since calculations with different MP grids are not fully comparable, the energies of the clean metal surface, $E^{tot}_{Pd(100)}$, and of bulk palladium, E^{tot}_{Pd}, needed to evaluate the Gibbs free energy of adsorption as defined in Eq. (2), have been calculated each time in the same supercell as the corresponding adlayers or surface oxide structures. The energy cutoff for the expansion of the wave function in the interstitial is $E^{wf}_{max} = 20$ Ry and for the potential $E^{pot}_{max} = 196$ Ry. Using these basis-set parameters the average binding energies per oxygen atom and CO molecule are converged within 50 meV, so that the Gibbs free energies of adsorption are converged within $1–5$ meV/Å^2.

All molecular calculations are done in rectangular supercells with side lengths of $(13 \times 14 \times 15)$ bohr (atoms) or $(13 \times 14 \times 20)$ bohr (molecules) using only the Γ-point to sample the BZ. To obtain very accurate values of the binding energies of the three gas phase molecules O_2, CO, and CO_2, the cutoff for the expansion of the wave function in the interstitial has been increased to $E^{wf}_{max} = 37$ Ry. With respect to this cutoff the binding energies are converged within $10–20$ meV.

The exchange-correlation (xc) energy is treated within the generalized gradient approximation (GGA) using the PBE[24] xc functional. To assess the error introduced to the total energies by the approximate xc energy, the most important calculations have also been repeated using another gradient-corrected xc functional, the RPBE,[25] as well as the LDA.[26] The influence of these different xc functionals on the results will be discussed below.

III. O AND/OR CO ADSORPTION AT Pd(100)

In this section we discuss the different adlayer structures of oxygen and/or CO on Pd(100) that will be compared within the constrained thermodynamic equilibrium approach. In addition to the on-surface adsorption of O/CO on Pd(100), the formation of a reconstructed $(\sqrt{5} \times \sqrt{5})R27°$ (abbreviated with $\sqrt{5}$ in the following) surface oxide has experimentally been observed at higher oxygen exposure.[27–30] Since the structure of the $\sqrt{5}$ surface oxide is quite different from the clean Pd(100) surface, also exhibiting different adsorption sites, we will discuss the two surfaces separately.

A. Adlayers on Pd(100)

1. Pure oxygen adsorption

Experimentally, four different adsorption structures have been observed when exposing the Pd(100) surface to

TABLE II. Calculated binding energies of on-surface adlayers of O/CO on Pd(100). For the pure adlayer structures the binding energies are given per O atom and CO molecule, respectively. For the mixed structures the total binding energies are given. All values are in eV.

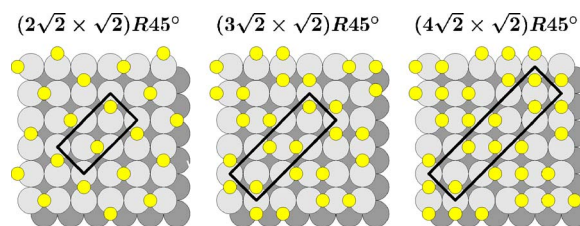|	Coverage Θ	E^{bind}
Pure O structures		
$p(2\times2)$-O^{hol}	0.25	-1.35
$c(2\times2)$-O^{hol}	0.50	-1.10
Pure CO structures		
$p(2\times2)$-CO^{br}	0.25	-1.92
$c(2\times2)$-CO^{br}	0.50	-1.92
$(2\sqrt{2}\times\sqrt{2})R45°$-CO^{br}	0.50	-1.92
$(3\sqrt{2}\times\sqrt{2})R45°$-CO^{br}	0.67	-1.73
$(4\sqrt{2}\times\sqrt{2})R45°$-CO^{br}	0.75	-1.63
(1×1)-CO^{br}	1.00	-1.31
Mixed O/CO structures		
(2×2)-O^{hol}-CO^{br}	0.50	-2.95
(2×2)-2O^{hol}-CO^{br}	0.75	-2.93
(2×2)-O^{hol}-2CO^{br}	0.75	-3.96
(2×2)-2O^{hol}-2CO^{br}	1.00	-3.64

FIG. 1. (Color online) Top views of the three experimentally characterized adlayer structures of CO on Pd(100). From left to right the coverage increases from $\Theta=0.5$ to $\Theta=0.67$ and $\Theta=0.75$ ML. The yellow small spheres represent the CO molecules, the gray large spheres the Pd(100) surface (second layer atoms are darkened).

oxygen.[27–31] These are a $p(2\times2)$, a $c(2\times2)$, a (5×5), and the $\sqrt{5}$ surface oxide structure. The $\sqrt{5}$ surface oxide will be discussed in detail in the next section. The (5×5) structure will not been considered in this study, since the structure and state of the oxygen atoms have not been well established so far, i.e., there exists no well-defined structural model. In addition, the (5×5) structure appears to be only of metastable character and its formation was found to be very sensitive to the surface preparation and oxygen exposure range, so that in the oxidation as well as in the reduction process the (5×5) structure can be bypassed, going directly from a (2×2) to a $\sqrt{5}$ structure and vice versa.[30]

This leaves as ordered adlayers only the $p(2\times2)$ at 0.25 monolayer (ML) coverage and the $c(2\times2)$ at 0.5 ML. Computing the binding energy of O atoms in all high-symmetry sites offered by the (100) surface (bridge, top, and hollow), we find in both structures the fourfold hollow site to be the most stable adsorption site. The binding energies are calculated with respect to the O$_2$ gas phase molecule [cf. Eq. (4)], and the values of the binding energies per oxygen atom are listed in Table II. It can be seen that the binding energy decreases going from the $p(2\times2)$ to the higher-coverage $c(2\times2)$ adlayer, indicating overall repulsive interactions between the adsorbed oxygen atoms.

2. Pure CO adsorption

The adsorption of CO on Pd(100) has been studied intensively.[32–39] In all experimental studies it is found that CO binds upright in the bridge position via the C atom. At a coverage of $\Theta=0.50$ ML an ordered $(2\sqrt{2}\times\sqrt{2})R45°$ adlayer is formed, which is compressed to a $(3\sqrt{2}\times\sqrt{2})R45°$ structure at $\Theta=0.67$ ML and a $(4\sqrt{2}\times\sqrt{2})R45°$ at $\Theta=0.75$ ML

(cf. Fig. 1). The formation of the $(2\sqrt{2}\times\sqrt{2})R45°$ adlayer rather than a simple $c(2\times2)$ structure is assumed to be mainly due to overall strongly repulsive interactions among the adsorbed CO molecules.[40]

In addition to these experimentally observed structures also simple (1×1) and (2×2) adlayers with CO in top, bridge, and hollow sites are considered in this work. The adsorption in bridge sites is found to be energetically favored at all computed coverages. Table II compiles therefore only the results for bridge-bonded CO. Looking at the values in Table II it can be seen that the binding energy per CO molecule is almost constant up to a coverage of $\Theta=0.50$ ML. For higher coverages the binding energy decreases due to overall repulsive interactions between the adsorbed CO molecules. Comparing the two discussed structures with a coverage of $\Theta=0.50$ ML we in fact find them to be degenerate within our computational accuracy (the $(2\sqrt{2}\times\sqrt{2})R45°$ is only favored by a few meV). These results are also fully consistent with previous DFT pseudopotential studies.[25,40]

3. Mixed O/CO adsorption

As to the adsorption of oxygen and CO on the Pd(100) surface, experimentally no ordered overlayers have been reported so far. If the Pd(100) surface is exposed to both oxygen and CO, the two adsorbed species tend to form separate domains instead.[31] In their low-energy electron diffraction (LEED) measurements Stuve et al.[31] observed that for a fully developed $p(2\times2)$-O/Pd(100) structure the $p(2\times2)$ LEED pattern vanished after exposure to CO at a temperature of $T=80$ K. Assuming a barrier of ≈1.0 eV for the reaction of O and CO to form CO$_2$,[41,42] it is rather unlikely that the adsorbed oxygen reacted with the CO at this low temperature. The disappearance of the LEED signal was thus interpreted as a CO-induced disordering of the oxygen islands. To nevertheless obtain an idea about the simultaneous adsorption of O and CO on Pd(100) we set up different models for mixed overlayer structures that seemed to be most obvious from a combinatorial point of view. For this we used (2×2) surface unit cells placing one to two O atoms and CO molecules in their favorite adsorption sites—i.e., O in hollow and CO in bridge sites. Excluding any structures where O and CO are closer to each other than the length a of the (1×1) surface unit cell we obtain the four different struc-

(2x2) - top view

O^{hol}-CO^{br} $2O^{hol}$-CO^{br} O^{hol}-$2CO^{br}$ $2O^{hol}$-$2CO^{br}$
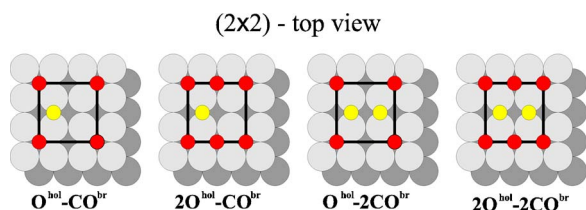
FIG. 2. (Color online) Top views of the considered coadsorbed overlayer structures of oxygen and CO on Pd(100). The small red (dark) spheres correspond to oxygen atoms, the small yellow (light) spheres the CO molecules, and the large gray spheres the Pd(100) surface (second layer atoms are darkened).

tures shown in Fig. 2. The corresponding average binding energies calculated using Eq. (3) are listed in Table II.

Similar to the pure adlayer structures of O or CO on Pd(100), the binding energy per adsorbate decreases with increasing coverage in the considered coadsorption structures. This trend in binding energies reflects the aforementioned repulsive interactions among the adsorbed O atoms and CO molecules. For a coverage of $\Theta=0.50$ ML the binding energy of the mixed O/CO overlayer is less favorable by 70 meV than the sum of the binding energies of the respective $c(2\times2)$ pure adlayers of O and CO. This indicates that the repulsive interactions among adsorbed O and CO are even stronger than between O, O and CO, CO, respectively, in the pure adlayer structures. At finite temperatures configurational entropy would tend to counteract the repulsive interactions, but in the temperature range discussed here this entropy contribution is rather small. The adsorption of both O and CO in hollow sites in a $c(2\times2)$ structure further decreases the binding strength of the adsorbates.

The even stronger repulsive interactions in these mixed adsorbate structures will thus favor the separation of oxygen and CO into separate domains. The adsorption of CO into a $p(2\times2)$-O structure can then induce a demixing of the two species and destroy the long-range order, which is consistent with the disappearance of the LEED spot intensities in the aforementioned experiment by Stuve et al.[31]

B. O and CO on the surface oxide

At a coverage of $\Theta=0.80$ ML, the adsorbed oxygen induces a reconstruction of the Pd(100) surface forming the $\sqrt{5}$ surface oxide structure. An atomistic model for the surface oxide (cf. Fig. 3) was proposed in a detailed experimental and theoretical study, revealing that the structure can actually be described as a PdO(101) trilayer on Pd(100).[43] The surface unit cell contains four palladium and four oxygen atoms. Two Pd atoms are fourfold and the other two are twofold coordinated by oxygen. There are also two kinds of O atoms. Two O atoms sit on top of the reconstructed Pd layer and two at the interface to the Pd(100) substrate forming the aforementioned trilayer structure.

In addition to the previous discussion on this surface oxide structure,[43] we note that the potential energy surface for a registry shift of the entire surface oxide trilayer over the Pd(100) substrate is very shallow. In particular, shifts of up to ~0.5 Å along the direction as indicated by the arrow in
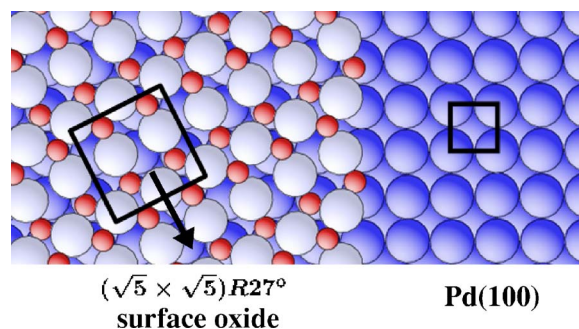

$(\sqrt{5}\times\sqrt{5})R27°$
surface oxide   **Pd(100)**

FIG. 3. (Color online) Top view of the $(\sqrt{5}\times\sqrt{5})R27°$ surface oxide structure (left part) and the Pd(100) substrate (right part) and their corresponding surface unit cells (black lines). Red small spheres represent the lattice oxygen atoms, large light-blue ones the reconstructed Pd atoms, and large dark-blue spheres Pd atoms belonging to the underlying Pd(100) substrate. The arrow indicates the easy shift direction of the surface oxide trilayer along the Pd(100) substrate.

Fig. 3 and parallel to the surface lead only to energy variations of less than 50 meV per $\sqrt{5}$ surface unit cell. Without anchoring by, e.g., defects, the lateral position of the ideal surface oxide over the Pd(100) surface is thus not well defined. In extended test calculations, we verified that this uncertainty in the lateral position has no consequence on the adsorption energetics discussed here and therefore simply used in the present work the lateral position determined in Ref. 43.

For the additional adsorption of oxygen and/or CO on the surface oxide structure, there are several possibilities. As can be seen in Fig. 4, the surface oxide exhibits top, bridge, and hollow high-symmetry sites. Due to the symmetry of the underlying Pd(100) substrate, multiple adsorption sites of the same type (top, bridge, or hollow) are not fully equivalent, but still very similar. Only the top sites differ substantially depending on whether the corresponding Pd atom is twofold or fourfold coordinated by oxygen. As yet there is no experimental information available for the additional adsorption of O or CO on the $\sqrt{5}$ surface oxide. Therefore, we performed a systematic investigation of possible overlayer structures of O and CO involving the reconstructed $\sqrt{5}$ surface oxide and starting with the adsorption sites depicted in Fig. 4.

In a first step only one CO molecule is adsorbed in any of the ten adsorption sites. We find that the four different hol-
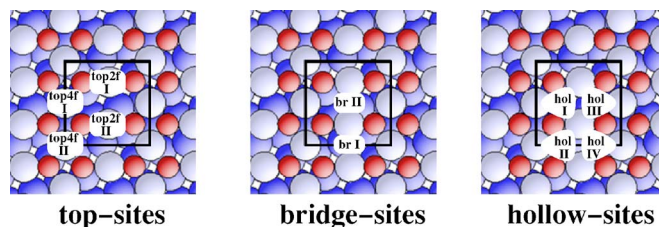

top−sites   **bridge−sites**   **hollow−sites**

FIG. 4. (Color online) Top views of high-symmetry adsorption sites on the $(\sqrt{5}\times\sqrt{5})R27°$ surface oxide structure. Red small spheres represent the lattice oxygen atoms, large light-blue ones the reconstructed Pd atoms, and large dark-blue spheres Pd atoms belonging to the underlying Pd(100) substrate.

TABLE III. Calculated binding energies of CO on the $\sqrt{5}$ surface oxide structure calculated using Eq. (5). 2CO denotes that two CO molecules are adsorbed in the $\sqrt{5}$ surface unit cell. The adsorption of two CO molecules in top4f sites or one CO in bridge and a second in a top2f site does not lead to a stable structure. All values are per CO molecule and in eV.

	$E_{CO@\sqrt{5}}^{bind}$		$E_{CO@\sqrt{5}}^{bind}$		$E_{CO@\sqrt{5}}^{bind}$
CO^{br}	−0.93	$2CO^{br}$	−0.75	$2CO^{br,top2f}$	−
CO^{top2f}	−0.62	$2CO^{top2f}$	−0.51	$2CO^{br,top4f}$	−0.45
CO^{top4f}	−0.13	$2CO^{top4f}$	−	$2CO^{top2f,top4f}$	−0.29

low sites are not stable, i.e., upon relaxation the adsorbed CO molecule always moves to the respective neighboring bridge site. The binding energies of the two bridge (br I and br II) sites are almost degenerate as expected from the only slight structural differences, i.e., the binding energies as defined in Eq. (5) differ by less than 0.1 eV. Similarly, the two top sites at the two twofold (top2f I and top2f II) oxygen coordinated Pd atoms exhibit nearly equivalent binding energies (ΔE^{bind} <50 meV). The same is also found for the two top sites at the two fourfold (top4f I and top4f II) oxygen coordinated Pd atoms. In the following we will thus treat these correspondingly very similar sites as being identical. The bridge site is the most stable adsorption site followed by the top2f site, and on the top4f site the CO molecule is already only weakly bound (cf. Table III).

It is also possible to adsorb two CO molecules in the $\sqrt{5}$ surface unit cell, and again we find the adsorption in the two bridge sites most stable. Mixing the adsorption sites—i.e., placing, e.g., one CO in a bridge site and a second one in a top 2f site—does always yield less stable structures than the adsorption in like sites (cf. Table III). It also becomes energetically very unfavorable to place more than two CO molecules in the $\sqrt{5}$ surface unit cell as deduced from test calculations with up to four CO molecules per surface unit cell.

The adsorption of oxygen in the high-symmetry sites of the $\sqrt{5}$ surface oxide gives similar results. Again, the bridge site is the most stable site ($E_{O@\sqrt{5}}^{bind}$=−0.14 eV) and the hollow sites are unstable upon relaxation. However, it is now not possible to adsorb any oxygen in the top2f and top4f sites in the $\sqrt{5}$ unit cell. If one CO molecule and one O atom are adsorbed simultaneously, likewise the adsorption in two bridge sites is found to be favored.

Our calculations with one and two adsorbates per $\sqrt{5}$ surface unit cell thus indicate noticeable overall repulsive lateral interactions. We correspondingly extended our calculations also to more sparse adlayers in (2×1) and (1×2) $\sqrt{5}$ surface unit cells, but did not find significant lateral interactions extending across the $\sqrt{5}$ surface unit cell. The obtained binding energies were always to within 25 meV per adsorbate of those calculated for the same adsorption site in a (1×1) cell.

To increase the configuration space of considered overlayers based on the $\sqrt{5}$ surface oxide, we also considered structures in which the original surface oxide structure is slightly modified. In a first step, one of the upper hollow site oxygen atoms is removed, and CO and O are again placed in the aforedescribed sites. Also in this modified structure the

bridge site results as the preferred adsorption site. If both upper oxygen atoms are removed from the $\sqrt{5}$ surface oxide, we find the structure already to some extend destabilized. Due to the lower palladium density in the reconstructed layer (four Pd atoms on five Pd(100) substrate atoms per unit cell) the structure is rather open, and structural relaxation showed that the Pd atoms can now move quite easily in lateral direction on the surface. It is still possible to adsorb O/CO in any of the other adsorption sites, but we found these structures either unstable upon relaxation or in general much less stable than the corresponding structures, where the original O hollow vacancy is refilled.

In addition to simply removing the upper oxygen atoms from the $\sqrt{5}$ surface oxide structure and filling additional on-surface adsorption sites, we also substituted the topmost O atoms by CO molecules and placed additional O atoms and/or CO molecules in top2f, top4f, and bridge sites. In the substituted hollow site the CO binds quite strongly. However, since the O atoms bind even stronger to this site by 0.6 eV, O will always preferentially occupy the hollow sites when the two adsorbates compete for this sites. The situation is reversed for adsorption in the bridge sites. Regardless of whether O or CO occupies the threefold hollow sites, we always find a stronger binding by at least 0.7 eV of CO compared to O at these bridge sites.

Even if we leave out the four unstable hollow sites in Fig. 4, there is finally still a huge amount of possible overlayer structures that can be created by combinatorially placing an arbitrary number of O and CO per surface unit cell into any of the available sites. Since there is only little known about the adsorption on the surface oxide, none of these structures can be excluded *a priori*. Motivated by the strong repulsive interactions seen in our calculations with one or two adsorbates per surface unit cell, we nevertheless discard quite a number of these structures with the criterion that no two adsorbates may sit in directly neighboring sites (i.e., at a distance of less than 1/4 of the length of $\sqrt{5}$ surface unit cell). This still leaves 92 "plausible" structures, and DFT calculations were performed for all of them (for more details on the calculated overlayer structures see Ref. 44). Out of these only 55 are stable upon relaxation and are then considered in our constrained "phase diagram."

IV. STABILITY IN A CONSTRAINED EQUILIBRIUM WITH AN O$_2$ AND CO GAS PHASE

Using the Gibbs free energy of adsorption as defined in Eq. (2) it is possible to compare the stability of all calculated adsorption structures in a constrained equilibrium with an O$_2$ and CO gas phase. In this approach the surface is considered to be in equilibrium with two separate gas phase reservoirs of O$_2$ and CO, i.e., the formation of CO$_2$ is neglected in the gas phase as well as at the surface.[16] In the gas phase this assumption seems quite justified, since the direct reaction of O$_2$ and CO is kinetically hindered by a huge free energy barrier. At the surface, though, the reaction is actually supposed to take place at the working catalyst. Here, the assumption of a constrained equilibrium is thus only reasonable as long as the O$_2$ and CO adsorption and desorption
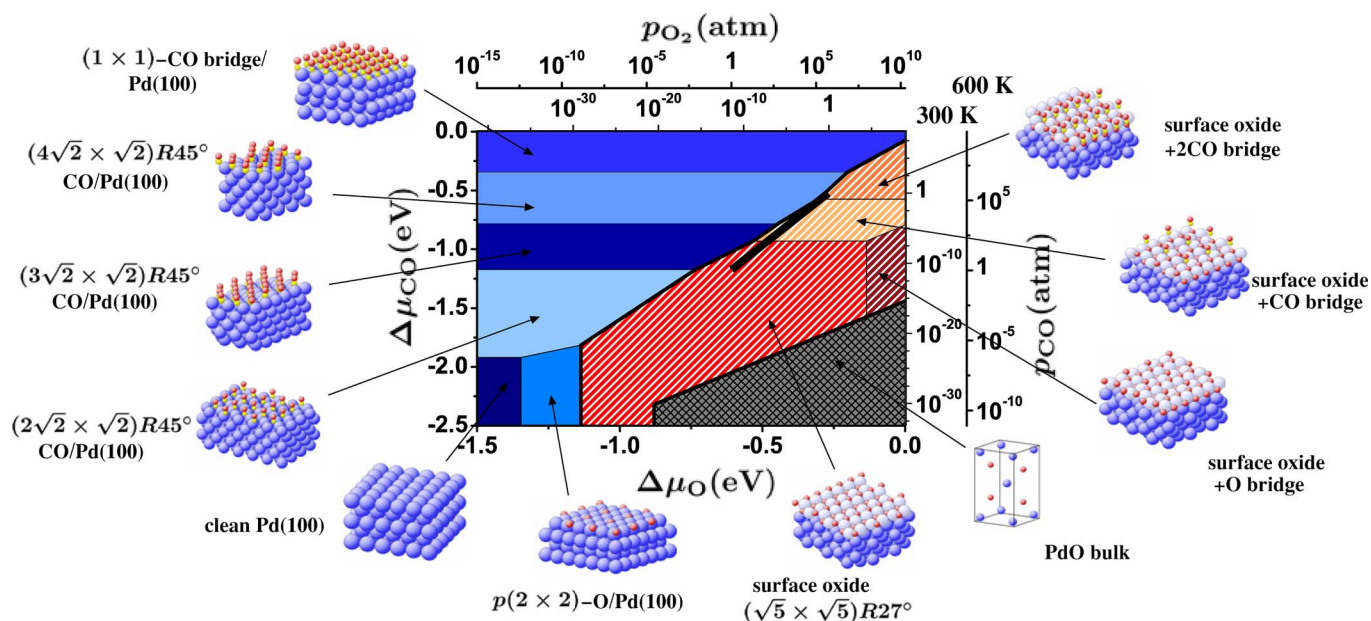
FIG. 5. (Color online) Surface "phase diagram" of the Pd(100) surface in constrained thermodynamic equilibrium with an O_2 and CO gas phase. The atomic structures underlying the various stable (co)adsorption structures on the metal and the surface oxide, as well as a thick bulklike oxide film (indicated by the bulk unit cell), are also shown (Pd=large blue spheres, O=small red spheres, and C=small yellow spheres). The black bar marks gas phase conditions representative of technological CO oxidation catalysis—i.e., partial pressures of 1 atm and temperatures of 300–600 K. The dependence of the chemical potentials of the two gas phases is translated into pressure scales for T =300 K and T=600 K (upper x axes and right y axes).

events are much more frequent than the reaction, so that the surface can maintain its equilibrium with the two gas phase components. In other words, the approach amounts to assuming that the kinetics of the ongoing catalytic reactions does not change the surface structure and composition. The resulting constrained surface "phase diagram" can thus only provide a first idea of the possibly relevant surface structures, which needs to be scrutinized explicitly treating the surface kinetics. On the other hand, the constrained equilibrium approach allows one to rapidly screen a huge number of (structurally quite different) surface configurations and compare their stability over a wide (T,p) range of possible gas phase conditions. By using *ab initio* thermodynamics we are thus able to identify those regions in (T,p) space that are likely catalytically active and where we then zoom in with more sophisticated methods. This second, refining step explicitly includes the effect of the reaction kinetics on the average surface composition (using kinetic Monte Carlo simulations), and the results of these simulations, which are restricted to the most relevant surface structural models identified here, are discussed in a second paper. This will then also bring us into a position to scrutinize the validity of the assumption of the constrained equilibrium approach employed here.

A. Surface phase diagram

The results of the above-described calculations concerning the aforediscussed overlayers of oxygen and CO on Pd(100), also including the (modified) $\sqrt{5}$ surface oxide structure, are summarized in Fig. 5, which shows the most stable "phases" (i.e., the ones that maximize ΔG^{ads} as defined

in Eq. (2)) for any given chemical potential of the oxygen and CO gas phases. The dependence on the chemical potentials has also been converted into more intuitive pressures scales for temperatures of T=300 K and T=600 K in the top two x axes for oxygen and the right two y axes for CO. As expected from the Gibbs phase rule, stable "phases" cover volumes in the three-dimensional space spanned by (T,p_{O_2},p_{CO}) and coexistence regions between two "phases" cover areas. Correspondingly in the two-dimensional sectional plane shown in Fig. 5 this leads to areas and lines for the two cases, respectively. Out of the set of 191 tested structures only 11 turn out to be "phases" appearing in Fig. 5.

We will start the discussion of the obtained constrained surface "phase diagram" in Fig. 5 in the lower left corner. Here, both the chemical potential of oxygen and CO are very low, i.e., the oxygen and CO content in the gas phase is insignificant and consequently the clean Pd(100) surface results as the most stable system state. If we now move along the x axis in Fig. 5 to the right, we reach more and more oxygen-rich conditions, while the CO content in the gas phase is kept low. The increase in the oxygen chemical potential leads to a stabilization of oxygen-containing structures with increasing coverage: First, the $p(2\times2)$-O overlayer on Pd(100),[45] then the $\sqrt{5}$ surface oxide, and finally the PdO bulk oxide representing thick bulklike oxide films on the surface. This sequence of stable structures was also confirmed by *in-situ* surface x-ray diffraction measurements.[4] Interestingly, the $c(2\times2)$ structure observed under UHV conditions[27–31] does not appear in the surface "phase diagram." Thus we conclude that the $c(2\times2)$ structure is most likely a metastable state produced by the exposure kinetics.

If the oxygen content is kept low in the gas phase and the CO content is gradually increased—i.e., moving from the lower left corner along the y axis to the top in Fig. 5—a series of ordered CO adlayer structures with increasing coverage is stabilized on Pd(100). At first we find the also experimentally observed $(2\sqrt{2}\times\sqrt{2})R45°$, $(3\sqrt{2}\times\sqrt{2})R45°$, and $(4\sqrt{2}\times\sqrt{2})R45°$ structures and, finally, for a very high CO content in the gas phase a (1×1) structure with 1 ML CO in bridge sites.

Starting again in the lower left corner of Fig. 5 we now move along the diagonal, which corresponds to increasing both the oxygen and CO content in the gas phase. Intuitively, one would expect coadsorption structures of O and CO on Pd(100) to become favorable. But none of the above-discussed ordered coadsorption structures (cf. Fig. 2) are found to be a most stable "phase" under any gas phase conditions. This is consistent with the already mentioned experimental findings, that O and CO prefer to form separate domains rather than ordered coadsorbed overlayers.[31] The lower stability of such mixed structures can be explained by the strongly repulsive interactions between adsorbed O and CO, which lead to a significant decrease in binding energies (cf. Table II). However, we can of course not exclude that ordered arrangements with different periodicities than those considered here would not lead to a lowering in the repulsive interactions. To take a reasonable part in the "phase diagram," though, the binding energies would have to increase by as much as 0.3–0.5 eV per O atom/CO molecule compared to the now proposed structures. Compared to the pure overlayer structures this would even imply the necessity of attractive interactions between the two species.

For high oxygen and CO content in the gas phase (upper right part of Fig. 5) we find instead coadsorbed structures involving the $\sqrt{5}$ surface oxide (two orange-white hatched regions) to become stable. These two mixed structures correspond to the surface oxide with one and two CO molecules adsorbed in bridge sites, respectively. In a small range of very oxygen-rich and intermediate CO gas phase conditions additional O adsorption in the bridge sites of the $\sqrt{5}$ structure leads also to a stable "phase" (dark red-white hatched region).

Looking again at the whole surface "phase diagram" in Fig. 5 the 11 "phases" can be divided into three groups: on-surface adlayer structures of O or CO on Pd(100), phases involving the $\sqrt{5}$ surface oxide structure, and the stability region of the bulk oxide as discussed in Sec. II B. Focusing on these three different groups of phases two important conclusions with respect to the relevance of oxide formation under catalytic reaction conditions can be drawn. First, the formation of a thick, bulklike oxide (gray cross hatched area) at the surface under technologically relevant gas phase conditions of O_2 and CO (black bar in Fig. 5, $p_i \sim 1$ atm, $T \sim 300-600$ K) can be ruled out. This is thus in marked contrast to the much wider stability range of bulk RuO_2, which does extend to these conditions.[18] Second, the stability region of the $\sqrt{5}$ surface oxide (hatched area) does extend to such conditions. In fact, it is either this monolayer thin surface oxide or CO adlayers on Pd(100), which are neighboring "phases" around the catalytically active region in (T,p)

space. As can be seen in Fig. 5 the catalytically relevant conditions are actually right at the boundary between the $\sqrt{5}$ surface oxide structures and the CO overlayer structures on Pd(100). Small changes in the Gibbs free energy of adsorption causing a shift in this boundary could thus well affect the conclusion as to which is the most stable "phase" under these conditions. Apart from the assumption of a *constrained* thermodynamic equilibrium, the main uncertainties, which may cause such changes in ΔG^{ads}, are the approximate DFT total energies and the neglected free energy contributions. We verified that the uncertainties in the DFT total energies due to the numerical approximations (supercell setup, finite basis set) are not significant in this respect. What needs to be scrutinized are therefore the uncertainties due to the approximate xc functional underlying the DFT total energies and the neglected free energy contributions to ΔG^{ads}. This will be done in the next two subsections.

B. Evaluating the Gibbs free energy

To calculate the Gibbs free energy of adsorption ΔG^{ads} the Gibbs free energies of the different components entering Eq. (2) have to be evaluated. The Gibbs free energy

$$G(T,p) = E^{\text{tot}} + F^{\text{vib}} - TS^{\text{conf}} + pV \qquad (9)$$

comprises contributions from the total energy E^{tot}, the vibrational free energy F^{vib} including the ZPE, the configurational entropy S^{conf}, and the pV term. In Eq. (2) we substituted the Gibbs free energy difference by only the leading term, the total energy differences, which can be directly obtained from DFT calculations. We assess the uncertainty introduced by this approximation by an order-of-magnitude estimate of the remaining contributions to ΔG^{ads}. If this first approximation reveals that the results are significantly influenced by considering all contributions to the Gibbs free energy, the respective terms have to be calculated explicitly. However, the order-of-magnitude estimate can be obtained very easily and is thus helpful to decide whether or not it becomes necessary to evaluate the entire Gibbs free energy.

Following the discussion in Refs. 13 and 16 the contributions to the Gibbs free energy of adsorption arising from the pV term and the configurational entropy are rather small for systems like the one presented here. We will thus only discuss the most crucial approximation: namely, the neglect of the vibrational free energy contribution, $\Delta F^{\text{ads,vib}}$ to the Gibbs free energy of adsorption. In order to estimate the size of $\Delta F^{\text{ads,vib}}$ we approximate the phonon density of states (DOS) within the Einstein model by one characteristic frequency. Following the approach outlined in Ref. 13 the vibrational contribution to the Gibbs free energy of adsorption for the $p(2\times2)$-O/Pd(100) structure can then be estimated as

$$\Delta F^{\text{ads,vib}}(T) \approx -\frac{1}{A}\left(F^{\text{vib}}(T,\overline{\omega}^{\text{surf}}_{\text{O-Pd}}) - \frac{1}{2}F^{\text{vib,ZPE}}(\overline{\omega}^{\text{gas}}_{\text{O}_2})\right), \qquad (10)$$

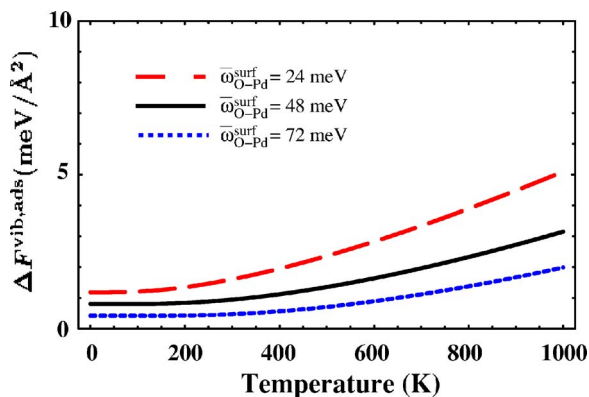where $F^{\text{vib}}(T,\omega)$ is the frequency-dependent function:

FIG. 6. (Color online) Vibrational contribution to the Gibbs free energy of adsorption for the $p(2\times2)$-O adlayer on Pd(100) within the Einstein approximation using different characteristic frequencies (see "inset" and text).

$$F^{\mathrm{vib}}(T,\omega) = \frac{1}{2}\hbar\omega + k_B T \ln(1 - e^{-\beta\hbar\omega}), \qquad (11)$$

with $\beta = 1/k_B T$. $\bar{\omega}_{\mathrm{O\text{-}Pd}}^{\mathrm{surf}}$ is the characteristic vibrational frequency of an oxygen atom adsorbed in a fourfold hollow site on Pd(100), and $\bar{\omega}_{\mathrm{O_2}}^{\mathrm{gas}}$ is the stretch frequency of the O_2 gas phase molecule. The change in the vibrational contribution of the Pd atoms in the clean and oxygen-covered Pd(100) is neglected, so that the vibrational contribution to ΔG^{ads} is given by the *difference* in the vibrational energy of the O_2 molecule in the gas phase and the oxygen atom on the surface. For the oxygen molecule only the ZPE (not included in the presented DFT total energies) has to be considered, since all remaining contributions to F^{vib} are already contained in $\Delta\mu_{\mathrm{O}}$ (cf. Eq. (2)). In Fig. 6 the resulting vibrational contribution $\Delta F^{\mathrm{ads,vib}}(T)$ is shown for a characteristic frequency of $\bar{\omega}_{\mathrm{O\text{-}Pd}}^{\mathrm{surf}} = 48$ meV for the Pd-O stretch frequency of an adsorbed O atom[46] and an O-O vibrational frequency of $\bar{\omega}_{\mathrm{O_2}}^{\mathrm{gas}} = 196$ meV.[47] We find that for the $p(2\times2)$-O/Pd(100) structure ($A_{(2\times2)} = 31.16$ Å^2) the vibrational contribution to ΔG^{ads} stays below ~3 meV/Å^2 for temperatures up to $T = 1000$ K (black solid line in Fig. 6). Since the chosen $\bar{\omega}_{\mathrm{O\text{-}Pd}}^{\mathrm{surf}}$ is only a rough guess, we also allow for a ±50% change of this value, but even then the contribution does not increase considerably (red dashed, −50%, and blue dotted, +50%, lines in Fig. 6).

Similar estimates have been performed for every structure considered for the surface "phase diagram" in Fig. 5. For CO-containing structures $\Delta F^{\mathrm{ads,vib}}$ comprises two different contributions when comparing the gas phase and the adsorbed state, namely, the change of the C-O stretch vibration due to the adsorption and an additional Pd-C vibration. For structures involving the $\sqrt{5}$ surface oxide ($A_{\sqrt{5}} = 38.95$ Å^2) an additional contribution arises from the change in the vibrational energy between bulk and surface Pd atoms. The $\sqrt{5}$ structure contains one surface atom fewer than the corresponding Pd(100) surface per unit cell which also has to be balanced by the bulk reservoir ($\Delta N_{\mathrm{Pd}} = -1$ in Eq. (2)).
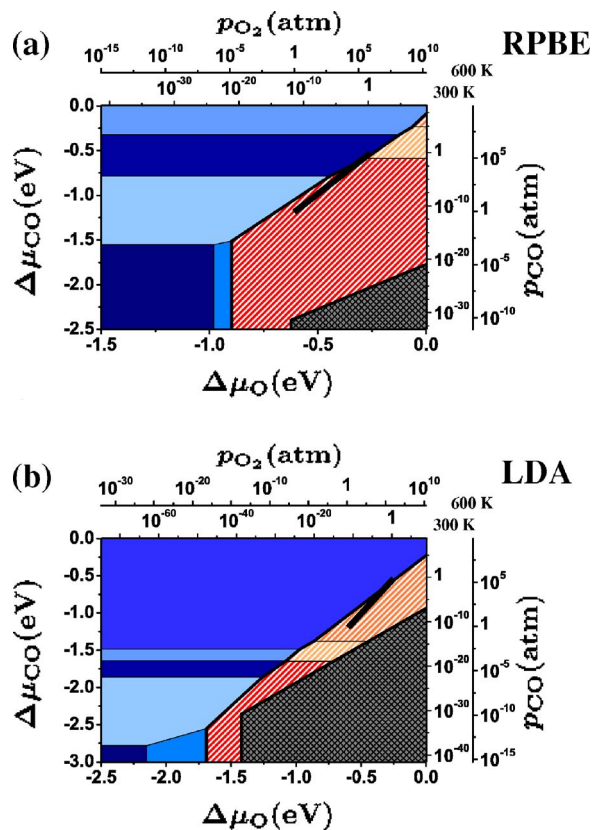

FIG. 7. (Color online) Surface "phase diagram" for the Pd(100) surface in a constrained equilibrium with an O_2 and CO gas phase. The top plot (a) shows the RPBE results and the bottom one (b) the LDA results. The color coding of the different "phases" is equivalent to the one used in Fig. 5. The black bar marks again gas phase conditions representative of technological CO oxidation catalysis— i.e., partial pressures of 1 atm and temperatures between 300 and 600 K. Note that the range of chemical potentials shown is larger for the LDA results, compared to the RPBE and the range in Fig. 5.

With this procedure we find that for all structures $\Delta F^{\mathrm{ads,vib}}$ stays always below 10 meV/Å^2 for temperatures up to $T = 600$ K. The surface "phase diagram" discussed in the previous section is not significantly changed if these estimated, maximum values for the vibrational contribution are included. There are some small shifts in the boundaries between stable "phases," but none of the stable structures disappears from and none of the unstable ones appears in the "phase diagram." Furthermore, the boundary between surface oxide structures and CO adlayers on Pd(100) is only marginally affected and consequently remains in the vicinity of the catalytic active region in (T,p) space. We are thus confident that for the results discussed here the approximation of the Gibbs free energy differences by only the total energy terms in Eq. (2) is justified.

C. Influence of the xc functional

To obtain an estimate of the uncertainty in Fig. 5 due to the choice of the PBE-GGA xc functional we reevaluate the

constrained surface "phase diagram" using the RPBE (Ref. 25) and LDA (Ref. 26) xc functionals. The corresponding surface "phase diagrams" are shown in Fig. 7 and are to be compared with Fig. 5. The "phase diagram" obtained by using the RPBE approximation for the xc energy (top graph, Fig. 7(a)) looks in fact very similar to the previously discussed one. There are some shifts in the actual "phase" boundaries, and the stability regions of the high-coverage phases of oxygen and CO, the $\sqrt{5}+O^{br}$ and (1×1)-CO^{br}/Pd(100) structures, are shifted outside the range of chemical potentials shown. Yet the overall topology is fully conserved. In agreement with the PBE results the bulk oxide is not a stable "phase" anywhere near ambient gas phase conditions. Due to the smaller heat of formation (cf. Table. I), the stability region of the bulk oxide is in fact much farther away from this region. Most importantly, the boundary between the simple overlayer structures on Pd(100) and the phases based on the $\sqrt{5}$ surface oxide structure (hatched area) is only very little influenced, so that the most interesting region for oxidation catalysis (black bar) is again right at the transition between a CO-covered Pd(100) surface and "phases" involving the surface oxide.

Even if the LDA is used as xc functional [bottom plot, Fig. 7(b)], the stability region of the bulk oxide does not extend to the catalytically relevant gas phase conditions. It covers a much larger range compared to the "phase diagrams" obtained using the two GGA functionals though. It should also be noted that in the shown LDA "phase diagram" the range of O and CO chemical potentials is enlarged to lower values to include the stability region of the clean metal surface, which in the LDA appears at much lower gas phase concentrations. This is a consequence of the strong overbinding in the LDA, which stabilizes any adsorbate structure at much lower pressures at the surface. Nevertheless, the range of technologically relevant catalytic gas phase conditions (black bar) lies again right at the boundary between the CO covered Pd(100) surface and $\sqrt{5}$ surface oxide structures.

From these results, we conclude that the choice of xc functional does have a strong influence on the absolute values of the binding energies and thereby also on the location of most of the phase boundaries in Figs. 5 and 7. However, particularly the boundary between the CO overlayer structures on Pd(100) and the $\sqrt{5}$ surface oxide is almost unchanged. The conclusion on the proximity of both phases to the catalytically relevant gas phase conditions seems therefore untouched by the uncertainty due to the approximate xc functional.

V. CONCLUSIONS

The stability of the Pd(100) surface has been investigated in a constrained thermodynamic equilibrium with a two-component gas phase consisting of O_2 and CO. In this approach the formation of CO_2 in the gas phase and at the surface is not considered, such that the effect of the surrounding gas phase on the surface structure and composition is modeled (as a first approximation) through contact with

independent reservoirs representing the reactants. To establish the actual surface "phase diagram" a large number of different structures with O and CO adsorbed in high-symmetry sites on the Pd(100) surface and on the $\sqrt{5}$ surface oxide structure have been considered. We find that under gas phase conditions of ambient temperatures and pressures, as applied in heterogeneous oxidation catalysis, it is either the nanometer thin surface oxide structure or a CO-covered Pd(100) surface that is stable, whereas the stability region of the bulk oxide does not extend to these gas phase conditions.[18]

To obtain an estimate of the uncertainty introduced by the choice of a specific xc functional the total energies entering the surface "phase diagram" have been calculated using the PBE, RPBE, and LDA. Comparing the "phase diagrams" for these three different xc functionals, partly dramatic shifts in the positions of the boundaries between the different stable "phases" can be observed. Yet it can also be seen that the position of the boundary between the CO-covered Pd(100) "phases" and the $\sqrt{5}$ surface oxide structures is in fact little affected. For all three xc functionals, the catalytically active region is very close to this boundary, but just still within the stability range of the surface oxide. We also verified that this finding is not affected by the numerical uncertainties and the free energy contributions neglected in our approach.

These results suggest that the only monolayer thin surface oxide structure might indeed be a relevant structure for the CO oxidation reaction on Pd(100) at technological relevant pressures. It has to be considered, though, that there are still two notable approximations in the constrained atomistic thermodynamics approach, as it has been applied here. First, configurational entropy is not included, and at finite temperatures a first effect would be to smear out the phase boundaries in the "phase diagram" and create coexistence regions, where the energetically low-lying configurations are mixed according to the law of mass action. At the phase boundary relevant for CO oxidation catalysis, this could, e.g., lead to the formation of coexisting domains of CO-covered Pd(100) and surface oxide patches. Second, the neglected kinetics of the ongoing catalytic CO_2 formation might significantly change the stability range of the different phases as obtained in the constrained equilibrium approach. A possible coexistence between patches of metallic Pd(100) covered by the reactants and patches of the surface oxide (possibly also with adsorbed CO) could then even under steady-state conditions go hand in hand with a continuous formation and decomposition of the oxidic phase. Such oscillations in the morphology of the catalyst surface could again significantly influence the catalytic function of this surface.

Based on the insight described in this paper we thus identify either the $\sqrt{5}$ surface oxide or CO-covered Pd(100) as surface structures most relevant under catalytically interesting gas phase conditions. It is therefore specifically the stability of the $\sqrt{5}$ surface oxide against CO-induced decomposition, which needs to be scrutinized to assess the active state of the surface under reaction conditions. In a second paper following the present one, we correspondingly extend our

study to investigate this stability. Using kinetic Monte Carlo simulations we then explicitly scrutinize the two major uncertainties of the present approach: namely, the effect of configurational disorder and the kinetic effects due to the ongoing reactions.

[1] N. W. Cant, P. C. Hicks, and B. S. Lennon, J. Catal. **54**, 372 (1978).

[2] H. Over and M. Muhler, Prog. Surf. Sci. **72**, 3 (2003).

[3] K. Reuter, Oil Gas Sci. Technol. **61**, 471 (2006); http://ogst.ifp.fr

[4] E. Lundgren, J. Gustafson, A. Mikkelsen, J. N. Andersen, A. Stierle, H. Dosch, M. Todorova, J. Rogal, K. Reuter, and M. Scheffler, Phys. Rev. Lett. **92**, 046101 (2004).

[5] B. L. M. Hendriksen, S. C. Bobaru, and J. W. M. Frenken, Surf. Sci. **552**, 229 (2004).

[6] B. L. M. Hendriksen, S. C. Bobaru, and J. W. M. Frenken, Catal. Today **105**, 234 (2005).

[7] E. Kaxiras, Y. Bar-Yam, J. D. Joannopoulos, and K. C. Pandey, Phys. Rev. B **35**, 9625 (1987).

[8] M. Scheffler, in *Physics of Solid Surfaces—1987*, edited by J. Koukal (Elsevier, Amsterdam, 1988).

[9] M. Scheffler and J. Dabrowski, Philos. Mag. A **58**, 107 (1988).

[10] G.-X. Qian, R. M. Martin, and D. J. Chadi, Phys. Rev. B **38**, 7649 (1988).

[11] X.-G. Wang, W. Weiss, Sh. K. Shaikhutdinov, M. Ritter, M. Petersen, F. Wagner, R. Schlögl, and M. Scheffler, Phys. Rev. Lett. **81**, 1038 (1998).

[12] X.-G. Wang, A. Chaka, and M. Scheffler, Phys. Rev. Lett. **84**, 3650 (2000).

[13] K. Reuter and M. Scheffler, Phys. Rev. B **65**, 035406 (2002).

[14] Z. Lodzianan and J. K. Nørskov, J. Chem. Phys. **118**, 11179 (2003).

[15] K. Reuter and M. Scheffler, Phys. Rev. Lett. **90**, 046103 (2003).

[16] K. Reuter and M. Scheffler, Phys. Rev. B **68**, 045407 (2003).

[17] W.-X. Li, C. Stampfl, and M. Scheffler, Phys. Rev. Lett. **90**, 256102 (2003).

[18] K. Reuter and M. Scheffler, Appl. Phys. A: Mater. Sci. Process. **78**, 793 (2004).

[19] A. Kiejna, G. Kresse, J. Rogal, A. De Sarkar, K. Reuter, and M. Scheffler, Phys. Rev. B **73**, 035404 (2006).

[20] *CRC Handbook of Chemistry and Physics: A ready-reference book of chemical and physical data*, edited by D. R. Lide and H. P. R. Frederikse, 76th ed. (CRC Press, Boca Raton, 1995).

[21] E. Sjöstedt, L. Nordström, and D. J. Singh, Solid State Commun. **114**, 15 (2000).

[22] G. K. H. Madsen, P. Blaha, K. Schwarz, E. Sjöstedt, and L. Nordström, Phys. Rev. B **64**, 195134 (2001).

[23] P. Blaha, K. Schwarz, G. K. Madsen, D. Kvasnicka, and J. Luitz, WIEN2k, Technische Universität Wien, Austria, 2001.

[24] J. P. Perdew, K. Burke, and M. Ernzerhof, Phys. Rev. Lett. **77**, 3865 (1996).

[25] B. Hammer, L. B. Hansen, and J. K. Nørskov, Phys. Rev. B **59**, 7413 (1999).

[26] J. P. Perdew and Y. Wang, Phys. Rev. B **45**, 13244 (1992).

[27] T. W. Orent and S. D. Bader, Surf. Sci. **115**, 323 (1992).

[28] S.-L. Chang and P. A. Thiel, J. Chem. Phys. **88**, 2071 (1988).

[29] S.-L. Chang, P. A. Thiel, and J. W. Evans, Surf. Sci. **205**, 117 (1988).

[30] G. Zheng and E. I. Altman, Surf. Sci. **504**, 253 (2002).

[31] E. M. Stuve, R. J. Madix, and C. R. Brundle, Surf. Sci. **146**, 155 (1984).

[32] A. M. Bradshaw and F. M. Hoffmann, Surf. Sci. **72**, 513 (1978).

[33] F. M. Hoffmann, Surf. Sci. Rep. **3**, 107 (1983).

[34] R. J. Behm, K. Christmann, G. Ertl, M. A. Van Hove, P. A. Thiel, and W. H. Weinberg, Surf. Sci. Lett. **88**, L59 (1979).

[35] R. J. Behm, K. Christmann, G. Ertl, and M. A. Van Hove, J. Chem. Phys. **73**, 2984 (1980).

[36] P. Uvdal, P.-A. Karlsson, C. Nyberg, S. Andersson, and N. V. Richardson, Surf. Sci. **202**, 167 (1988).

[37] K. Yoshioka, F. Kitamura, M. Takeda, M. Takahashi, and M. Ito, Surf. Sci. **227**, 90 (1990).

[38] J. N. Andersen, M. Qvarford, R. Nyholm, S. L. Sorensen, and C. Wigren, Phys. Rev. Lett. **67**, 2822 (1991).

[39] W. Berndt and A. M. Bradshaw, Surf. Sci. Lett. **279**, L165 (1992).

[40] A. Eichler and J. Hafner, Phys. Rev. B **57**, 10110 (1998).

[41] C. J. Zhang and P. Hu, J. Am. Chem. Soc. **123**, 1166 (2001).

[42] A. Eichler, Surf. Sci. **498**, 314 (2002).

[43] M. Todorova, E. Lundgren, V. Blum, A. Mikkelsen, S. Gray, J. Gustafson, M. Borg, J. Rogal, K. Reuter, J. N. Andersen, and M. Scheffler, Surf. Sci. **541**, 101 (2003).

[44] J. Rogal, Ph.D. thesis, Freie Universität Berlin, 2006; cf. Appendix B.1.

[45] We note that in our earlier calculations (Refs. 4 and 18) the $p(2 \times 2)$ overlayer did not appear as stable structure. The discrepancy between these earlier results and the data presented here is partly due to an improved convergence of the DFT calculations, as well as to an explicit treatment of the difference in the Pd atom density ($\Delta N_{Pd} \neq 0$) between the Pd(100) surface and the reconstructed $\sqrt{5}$ surface oxide, when calculating the Gibbs free energy of adsorption.

[46] C. Nyberg and C. G. Tengstål, Surf. Sci. **126**, 163 (1983).

[47] G. Herzberg, *Molecular Spectra and Molecular Structure I: Spectra of diatomic molecules*, 2nd ed. (Van Nostrand Reinhold, New York, 1950).